Frontiers in Bioscience Landmark

Front. Biosci. (Landmark Ed) **2025**; 30(5): 38875
https://doi.org/10.31083/FBL38875

Original Research

TNIK Regulates Cytoskeletal Organization to Promote Focal Adhesion Turnover and Mitosis in Lung Adenocarcinoma

Yao Li[1,†], Meng-yao Song[2,†], Xing Hu[1], Xue-hua Sun[1], Tao Zhang[1], Lu Zhang[1], Ying-xiong Wang[3], Qian Zhang[2], Chun-dong Zhang[1,*], Lian Zhang[4,*]

[1]Department of Biochemistry and Molecular Biology, School of Basic Medical Sciences, Chongqing Medical University, 400016 Chongqing, China
[2]Laboratory Animal Center, Chongqing Medical University, 400016 Chongqing, China
[3]The Joint International Research Laboratory of Reproduction and Development, Department of Reproductive Biology School of Public Health, Chongqing Medical University, 400016 Chongqing, China
[4]Department of Histology and Embryology, School of Basic Medical Sciences, Chongqing Medical University, 400016 Chongqing, China
*Correspondence: zhangcd@cqmu.edu.cn (Chun-dong Zhang); zhanglian@hospital.cqmu.edu.cn (Lian Zhang)
[†]These authors contributed equally.
Academic Editor: Esteban C. Gabazza
Submitted: 7 March 2025 Revised: 25 April 2025 Accepted: 6 May 2025 Published: 22 May 2025

Abstract

Background: Lung cancer is the primary cause of cancer-related mortality, but the molecular mechanisms behind this malignancy remain unclear. **Methods**: The Cancer Genome Atlas (TCGA) online database and tissue chips were used to analyze the expression levels of tumor necrosis factor receptor-associated factor 2 (TRAF2)- and non-catalytic region of tyrosine kinase adaptor protein (NCK)-interacting kinase (TNIK) protein in lung cancer. A549 and PC-9 lung adenocarcinoma (LUAD) cells with stable TNIK knockdown were generated by lentivirus infection. The tumor phenotypes were subsequently examined both *in vitro* and *in vivo*. The TCGA online database and RNA-sequencing of TNIK-knockdown cells were used to study the molecular mechanism underlying the TNIK-mediated phenotype of LUAD cells. The effects of TNIK knockdown on focal adhesion dynamics and mitosis were examined by indirect immunofluorescence and Western blot, on the sensitivity to chemotherapy drugs by cell counting kit-8 (CCK-8) assay, on apoptosis by flow cytometry, and on cell proliferation by 5-ethynyl-2′-deoxyuridine (EDU). **Results**: TNIK was highly expressed in LUAD ($p < 0.0001$), predominantly in the cytosol. Phenotype assays revealed that TNIK knockdown in LUAD cells led to a significant increase in cell spreading ($p < 0.0001$), but also inhibition of cell growth and movement ($p < 0.01$). Mechanistically, TNIK was found to regulate F-actin and microtubule organization, as well as the Ras homolog gene family (RHO)/RHO-associated kinase 2 (ROCK2)/LIM motif-containing protein kinase 1 (LIMK1) signaling pathway, thereby playing a crucial role in the control of focal adhesion turnover and mitosis. Additionally, the silencing of TNIK enhanced the sensitivity of LUAD cells to chemotherapeutic drugs. **Conclusions**: Our findings suggest that TNIK regulates focal adhesion turnover and mitosis to promote tumor malignancy via the RHO/ROCK2/LIMK1 pathway. The combination of TNIK targeting with chemotherapeutic drugs could be an effective strategy to overcome resistance in LUAD.

Keywords: TNIK; LIMK1; actins; microtubules; adenocarcinoma of lung

1. Introduction

Lung cancer is one of the most common malignancies and the leading cause of cancer-related deaths globally [1]. For the majority of these patients, chemotherapy is no longer the best treatment option. Future improvements are likely to come from better ways to combine immunotherapy, chemotherapy and targeted therapy through the identification of the tumors' molecular characteristics [2,3]. Therefore, acquiring a deeper understanding of the molecular mechanisms that underlie lung cancer should help in the development of more effective combination therapies.

Cells undergo changes in shape during movement and mitosis. In cancer cells grown in culture, flat and adherent cells during interphase and quiescence can transform into spherical and weakly adherent cells during mitosis and movement [4]. Focal adhesions (FAs) play an important role in regulating cell shape, migration, division and therapy resistance [5–7]. FAs are micron-sized, actin-based structures that connect cells to the extracellular matrix (ECM). They are made up of different signaling, catalytic (e.g., protein kinases, phosphatases, proteases), cytoskeletal, adaptor and scaffold proteins [8]. The key component of FAs is focal adhesion kinase (FAK), which is also present at other sites in the cell where it performs crucial tasks [9]. Nuclear localization of FAK has been demonstrated to enhance cancer cell survival [10]. The spatiotemporal modulation of FA dynamics is coordinated by actin–microtubule crosstalk [4]. Disruption of F-actin and microtubule organization can inhibit the disassembly of FAs, thereby disrupting downstream signaling [6,8]. Members of the Ras homolog gene family (RHO) family of small GTPases are key participants in actin–microtubule crosstalk. The best characterized RHO GTPases are RHO, Rac and Cdc42. LIM motif-containing protein kinase 1 (LIMK1) is a downstream signaling target of the RHO/RHO-associated

kinase (ROCK) pathway and is essential in cytoskeletal rearrangement by remodeling both actin filaments and microtubules [11,12].

Traf2- and Nck-interacting kinase (TNIK) is a member of the germinal center kinase (GCK) family. It is localized in the cytoplasm where it interacts with and phosphorylates cytoskeletal structures [13]. Human TNIK is comprised of three domains: a C-terminal region, an intermediate domain and an N-terminal kinase domain with the ATP-binding site. The latter serves as a target for the development of small-molecule inhibitors [14]. The C-terminal domain is known as the citron homology (CNH) domain, is conserved in GCK kinases, and has been shown to activate the c-Jun N-terminal kinase (JNK) pathway [15]. In addition, this domain regulates the actin cytoskeleton through its interaction with Rap2, a small GTPase member of the Ras family [16].

TNIK is an oncogenic "driver" kinase that has been targeted by several small inhibitors in a variety of cancer types [17–19]. Therefore, in the present work, we sought to investigate the role and underlying mechanisms by which TNIK regulates lung cancer development and progression, and to explore the potential of TNIK inhibition in combination with chemotherapy as a novel therapeutic strategy to enhance lung cancer treatment efficacy.

2. Materials and Methods

2.1 The Cancer Genome Atlas (TCGA) Analysis

The TCGA-lung adenocarcinoma (LUAD) (Firehose Legacy, 586 samples) and TCGA-lung squamous cell carcinoma (LUSC) (Firehose Legacy, 511 samples) reverse-phase protein array (RPPA) datasets were sourced from cBioPortal (https://www.cbioportal.org/) for Cancer Genomics. Samples with higher expression of TNIK protein as indicated by z-scores in RPPA were collected: 14 LUAD samples with high expression of TNIK, and 140 LUSC samples with high expression of TNIK. The gene expression profiles of LUAD and LUSC RNAseq (Firehose Legacy) were downloaded from xenabrowser.net (https://xenabrowser.net/datapages/). Gene set enrichment analysis (GSEA) (https://www.gsea-msigdb.org/gsea/index.jsp) was used to compare the mRNA profile of tumor tissues with high expression of TNIK in the RPPA to that of 59 adjacent normal samples.

2.2 Tissue Chip Analysis

Two tissue chips were purchased from Shanghai OUTDO Biotech: HLugA150CS03 containing 75 LUAD samples, and HLugS120CS01 containing 60 LUSC samples. Immunohistochemical (IHC) staining for TNIK (HPA0121128, 1:100 dilution, Sigma, St. Louis, MO, USA) was performed on the tissue chips, with Image-J software (version 1.48; National Institute of Health, Bethesda, MD, USA) used to measure the signal density. Integrated optical density (IOD) value/cell was calculated to quantify the IHC score. Shanghai OUTDO Biotech committees approved this study on clinical samples, and all applicable ethical regulations were followed (protocol code SHYJS-CP-1901006, approved on 1st January 2019 for HLugS120CS01; protocol code SHYJS-CP-1901005, approved on 1st January 2019 for HLugA150CS03).

2.3 Cell Culture

A549 cells were cultured in DMEM-F12 (SH30023.01, Hyclone, Waltham, MA, USA) and PC-9 cells in DMEM (SH30243, Hyclone) containing 10% heat-inactivated fetal bovine serum (FSP500, ExCell, Uruguay) and penicillin (100 IU/mL)/streptomycin (100 mf/mL) (SV30010, Hyclone). Cells were grown at 37 °C in a water-saturated atmosphere containing 5% CO_2. Both cell lines were validated by short tandem repeat (STR) profiling and tested negative for mycoplasma.

Two shRNA sequences of the *TNIK* gene (shT-1#: 5′-CCATCTCATATTCAGGGCAA-3′; shT-2#: 5′-GCCTCAAAGAACAACTTCTAT-3′) and a shRNA control sequence (shCtrl: 5′-TTCTCCGAACGTGTCACGT-3′) were designed and constructed into a plko.1-puro lentivirus vector (#8453, Addgene, Watertown, MA, USA). As per the manufacturer's instructions, 60%~70% of 293T cells in a 10 cm plate were transfected with either the control vector or *TNIK*-shRNA vector, along with Neofect™ DNA transfection reagent (TF20121201, NEOFECT, Beijing, China) to generate recombinant lentiviruses. Fresh culture medium was added to the cells 24 h after transfection. The cell supernatant was collected 48 h after transfection, concentrated using polyethylene glycol precipitation, filtered through 0.45 µm cellulose acetate filters (SLHV033RB, Merck Millipore, San Jose, CA, USA), and centrifuged for 40 minutes at 4 °C and 3500 rpm. For infection with lentivirus, A549 and PC-9 cells were first seeded at a density of 3×10^5 cells per well in 6-well plates and grown for 24 h. The culture fluid was then replaced with 1900 µL of fresh culture medium together with 100 µL of lentivirus particles (control or *TNIK*-shRNA). After 48 h, the supernatant was replaced with fresh medium containing 1 µg/mL of puromycin (A1113806, Thermo Fisher Scientific, Waltham, MA, USA) for six days to enable stable cell line selection.

Two siRNA sequences for *LIMK1* (siL-1#: 5′-CCATGGGTGCTCTGAGCAAAT-3′; siL-2#: 5′-GATCGTCCTGTGCGAGATCAT-3′) and two for *ROCK2* (siR-1#: 5′-GCACAGTTTGAGAAGCAGCTA-3′; siR-2#: 5′-GCCTTGCATATTGGTCTGGAT-3′) were designed (Shanghai GenePharma, Shanghai, China). The siRNAs were transfected into the indicated cells using Lipofectamine RNAiMAX reagent (13778150, Invitrogen, Waltham, MA, USA) according to the manufacturer's instructions. Cells were collected 48–72 h after transfection and subjected to analysis.

2.4 Clone Formation Assay and Cell Migration Trajectory Assays

For the clone formation assay, cells were resuspended at a density of 200 cells/mL in a single-cell suspension and 400 cells per well were then seeded into a 6-well plate. The cells were cultured for 14 days before being fixed in absolute ethanol for 10 min, followed by staining with 0.1% crystal violet (A600331, Sangon, Shanghai, China) for 30 minutes. Colonies with more than 50 cells were counted, and the relative number of colonies was calculated for each group.

For the cell migration trajectory assay, A549 and PC-9 cells were seeded (2×10^5 cells/well) in a 6-well plate. After 12 h, the cells were monitored using HoloMonitor M4 (Phase Holographic Imaging PHI AB, Skiffervägen, Lund, Sweden) and photographs were taken every 5 minutes for 20 minutes. The cell migration trajectory was analyzed with HoloMonitor software (Version 2.7.1, Phase Holographic Imaging PHI AB, Skiffervägen, Lund, Sweden).

2.5 EDU Labeling Assays

A total of 3×10^5 cells per well were seeded into a 24-well plate. After 24 h, the cells were labeled with 5-ethynyl-2′-deoxyuridine (EDU) using the Cell-Light EdU Apollo488 *In Vitro* Kit in accordance with the manufacturer's instructions (C10310-3, Ribobio, Guangzhou, China). Alternately, the cells were treated with chemotherapy drugs for 48 h prior to the EDU labeling. Finally, the cells were mounted with medium containing 4′, 6-diamidino-2-phenylindole (DAPI, D9564, 1:1000 dilution, Sigma) and viewed with a Leica confocal microscope (Leica Microsystems GmbH, Wetzlar, Germany).

2.6 Cell Morphology Analysis

Following stable TNIK knockdown, cells were photographed using a Leica light microscope (Leica SP8 Confocal Microscope, Wetzlar, Germany) at different locations on the coverslips (40× magnification). The single cell area was analyzed using Image-J software.

2.7 Mouse Experiments

Ten male BALB/c nude Mice (4–6 weeks old, 18–22 g) were purchased from Beijing Vital River Laboratory Animal Technology Co., Ltd. (Beijing, China). The mice were bred and housed in a specific pathogen-free (SPF) facility under controlled conditions: constant temperature (21 ± 0.5 °C), 12-hour light/dark cycle and 50% humidity. They had free access to autoclaved food and water, and were allowed a 7-day acclimation period before the start of experiments. Animal ethics approval for all experiments was obtained from the Chongqing Medical University Institutional Animal Care and Treatment Committee (Ethic Approval Number: IACUC-CQMU-2024-0593).

For tumor xenograft experiments, 6×10^6 A549 cells infected with lentivirus (control shRNA or TNIK-shRNA) were subcutaneously implanted into the right axillary region of male nude mice (4 mice per group). At 35 days after injection, the mice were anesthetized with 2% isoflurane and euthanized by cervical dislocation. Tumors were harvested, and their weight and volume were measured. The tumor size (width and length) was measured using a caliper, and the volume was computed as ($\text{width}^2 \times \text{length}$)/2 (expressed in mm^3) and weight was recorded in milligrams (mg). Harvested tumors were immediately fixed in 10% neutral-buffered formalin for subsequent analyses. Formalin-fixed tumors were embedded in paraffin, and 4-micrometer sections were analyzed for proliferating cell nuclear antigen (PCNA) by IHC (13110, 1:500 dilution, CST, Danvers, MA, USA).

2.8 RNA-sequencing Analysis

Cells with stable TNIK knockdown and control cells underwent RNA-seq analysis. Total RNA was extracted and sequencing was performed by BGI (Shenzhen, China). Differentially expressed genes (DEGs) were screened using the criteria of $|\log_2\text{fold change}| > 1$, and adjusted p-value < 0.05. Altered biological processes were identified using gene set enrichment analysis (GSEA).

2.9 Quantitative Reverse Transcription Polymerase Chain Reaction (qRT-PCR), Immunoblot and Immunofluorescence

Total RNA was isolated from lung cancer cells using trizol (15596026, Invitrogen). Next, reverse transcription was performed with 1 µg of RNA using the PrimeScript™ RT Master Mix (RR036A, Takara, Kusatsu, Shiga, Japan) in a 20-microliter reaction volume. Quantitative PCR was carried out using the SYBR Green qPCR Master Mix (B21202, Bimake, Houston, TX, USA). Gene expression was normalized to GAPDH and analyzed using the $2^{-\Delta\Delta CT}$ method. Primers were synthesized by BGI-Write (Beijing, China) and the primer sequences utilized in this study are presented in **Supplementary Table 1**.

For immunoblot experiments, the cells were lysed in RIPA buffer containing a protease inhibitor cocktail (B14001 and B15001, Bimake). The protein concentration in each lysate was measured, followed by denaturation at 100 °C for 5 min. Equal volumes of the lysates (30 µg of protein) were separated by 8% or 10% standard SDS-PAGE, and then electro-transferred onto polyvinylidene difluoride membranes (IPVH00010, Merck Millipore). The membranes were blocked with 5% non-fat dry milk in TBST at room temperature for 2 h, probed with the indicated primary antibodies at 4 °C overnight, followed by incubation with matching secondary antibodies at 37 °C for 2 h. The antibodies used for immunoblot were as follows: TNIK (HPA0121128, 1:1000 dilution, Sigma), RHOA (2117, 1:1000 dilution, CST), RHOB (2098, 1:1000 dilution, CST), ROCK1 (28999, 1:1000 dilution, CST), ROCK2 (47012, 1:1000 dilution, CST), LIMK1 (3842, 1:1000 dilution, CST), GAPDH (AB-P-R001, 1:1000 di-

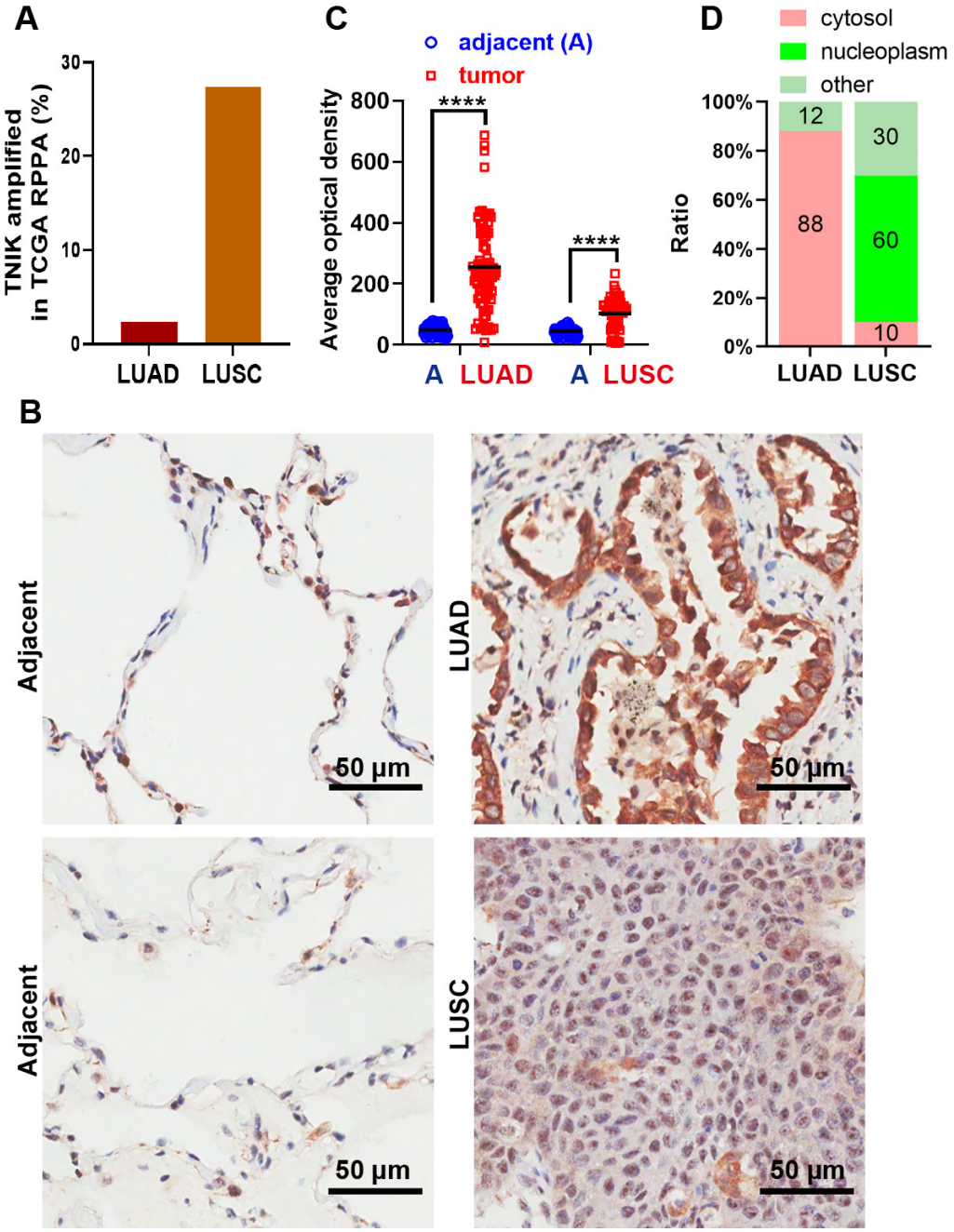

Fig. 1. Upregulation of TNIK protein is associated with the progression of LUAD. (A) The ratio of TNIK expression in the TCGA RPPA datasets for LUAD and LUSC. (B) Representative IHC staining of TNIK protein showing subcellular localization in adjacent normal tissue (left), LUAD (upper right) and LUSC (lower right). Scale bar, 50 μm. (C,D) Statistical analysis of TNIK expression and subcellular distribution in adjacent normal and tumor tissue of 75 LUAD and 60 LUSC cases. Cytosol: TNIK is mainly localized to the cytosol; nucleoplasm: TNIK is mainly localized to the nucleoplasm; others: no TNIK is expressed in either the cytosol or nucleoplasm. **** $p < 0.0001$. TNIK, Traf2- and Nck-interacting kinase; LUAD, lung adenocarcinoma; LUSC, lung squamous cell carcinoma; TCGA, The Cancer Genome Atlas; RPPA, reverse-phase protein arrays; IHC, immunohistochemical; A, adjacent normal tissue.

lution, Xianzhi Bio, Hangzhou, China), vinculin (V9264, 1:2000 dilution, Sigma), p-FAK^{397} (8556, 1:1000 dilution, CST) and FAK (3285, 1:1000 dilution, CST). The membranes were washed three times with Tris Buffered Saline with Tween (TBST) (10 min per wash) between antibody incubations. For secondary antibody incubation, horseradish peroxidase (HRP)-conjugated goat anti-rabbit IgG (H+L) (A0208, 1:1000 dilution, Beyotime, Shanghai, China) or goat anti-mouse IgG (H+L) (A0216, Beyotime, 1:1000 dilution) was used, depending on the species origin of the primary antibodies. The membranes were incubated with secondary antibodies at 37 °C for 2 h, followed

by three additional TBST washes (10 min each). Protein bands were visualized using an enhanced chemiluminescence (ECL) detection system.

For immunofluorescence, cells were fixed and then incubated with phalloidin–TRITC (P1951, 1:1600 dilution, Sigma), vinculin (V9264, 1:200 dilution, Sigma) or tubulin (AT819, 1:200 dilution, Beyotime). They were subsequently incubated with Alexa 488/568-conjugated secondary antibodies (A32766/A32790, 1:1000 dilution, Invitrogen) and then mounted with medium containing 4′,6-diamidino-2-phenylindole (DAPI, D9564, 1:1000 dilution, Sigma). A Leica confocal microscope was used to view the preparations.

2.10 In Vitro Cell Sensitivity for Chemotherapy Drugs

Cells with stable knockdown of TNIK and control cells were incubated with the chemotherapy agents paclitaxel (PTX) (S1150, Selleck, Houston, TX, USA), cisplatin (also known as cis-Diaminodichloroplatinum, DDP) (S1166, Selleck) and adriamycin (ADR) (S1280, Selleck) at the dosage and duration shown in the figure legend. Cell viability was then quantified by cell counting kit-8 (CCK-8) assay (B34304, Bimake, Houston, TX, USA). The optical density (OD) at 490 nm was measured using a microplate reader (51119100, Thermo, Waltham, MA, USA), and the 50% inhibition of cell proliferation (IC50) value was calculated with GraphPad Prism software (version 9; GraphPad Software, Boston, MA, USA).

2.11 Apoptosis Assay

Briefly, cells with stable knockdown of TNIK and control cells were incubated with chemotherapy agents for 48 h, stained with Annexin V-FITC and propidium iodide (PI) (MA0220, meilunbio, Dalian, China) for 30 minutes in the dark, and then analyzed by FACS.

2.12 Statistical Analysis

GraphPad Prism software was used for statistical analysis. Two-tailed Student's t test was used for the analysis and comparison of data from two groups. Statistical data were presented as the mean ± SEM. A p-value of <0.05 represents statistical significance. * indicates $p < 0.05$, ** indicates $p < 0.01$, *** indicates $p < 0.001$, and **** indicates $p < 0.0001$ ($p > 0.05$ refers to no significant difference).

3. Results

3.1 Upregulation of TNIK Protein Was Associated With the Progression of LUAD

To evaluate TNIK protein expression in lung cancer, we analyzed TNIK protein expression data obtained using reverse-phase protein array (RPPA) and available from The Cancer Genome Atlas (https://www.cbioportal.org). TNIK protein expression was found to be elevated in 2.3% of LUAD cases and 27.4% of LUSC samples (Fig. 1A). Next, we used IHC to evaluate TNIK protein expression in clinical samples of LUAD and LUSC. Tissue chip analysis revealed that TNIK protein expression was upregulated in both LUAD and LUSC samples compared to adjacent normal tissues ($p < 0.0001$, Fig. 1B,C). Interestingly, TNIK protein in LUAD was mainly localized in the cytoplasm, whereas TNIK in the adjacent normal tissues and in LUSC was mainly localized in the nucleus (Fig. 1B,D). Collectively, these results imply that TNIK is a positive regulator for LUAD progression and may have distinct effects on the development and progression of LUAD and LUSC. Previous research reported that upregulation of TNIK strengthens and maintains cell viability in LUSC [20], although the role of TNIK in LUAD has so far remained unclear.

3.2 TNIK Is Required for Maintaining the LUAD Malignant Phenotype In Vitro and In Vivo

To evaluate the role of TNIK in LUAD progression, we generated cells with stable TNIK knockdown using the two LUAD cell lines A549 and PC-9. The knockdown effects were verified by qRT-PCR and immunoblotting analysis ($p < 0.001$, Fig. 2A,B). Next, we examined whether TNIK affected LUAD cell proliferation by conducting colony formation and EDU labeling assays. The results showed that silencing of TNIK significantly inhibited the proliferation of A549 and PC-9 cells ($p < 0.01$, Fig. 2C–F). Furthermore, cell morphology analysis revealed that TNIK knockdown increased the area of cell spread ($p < 0.0001$, Fig. 2G,H). We then assessed the significance of TNIK on cancer cell movement. Cell migration assays showed that depletion of TNIK slowed the movement of A549 and PC-9 cells ($p < 0.01$, Fig. 2I,J). These findings indicate that *in vitro* proliferation and movement of LUAD cells are enhanced by TNIK expression. To determine whether TNIK can also regulate the growth of LUAD cells *in vivo*, A549 cells with a stable control vector or TNIK knockdown were subcutaneously injected into nude mice to enable tumor formation. As shown in Fig. 2K–M ($p < 0.001$), TNIK silencing greatly slowed the growth of xenograft tumors in mice compared to the control. IHC staining also confirmed that TNIK silencing inhibited PCNA expression ($p < 0.01$, Fig. 2N,O). Together, these findings show that TNIK is necessary to maintain the LUAD cell malignant phenotype, both *in vitro* and *in vivo*.

3.3 TNIK Regulates F-actin and Microtubule Cytoskeletal Organization via the RHO/ROCK2/LIMK1 Signaling Pathway

IHC analysis showed that TNIK was localized mainly in the cytoplasm of LUAD cells, but also in the nucleus. This indicates a critical function for cytoplasmic TNIK in the progression of LUAD. To study the molecular mechanism underlying the TNIK-associated malignant phenotype in LUAD, RNAseq analysis was performed to ascertain changes in the gene expression profile at the whole genome level in A549 cells with stable TNIK knockdown.

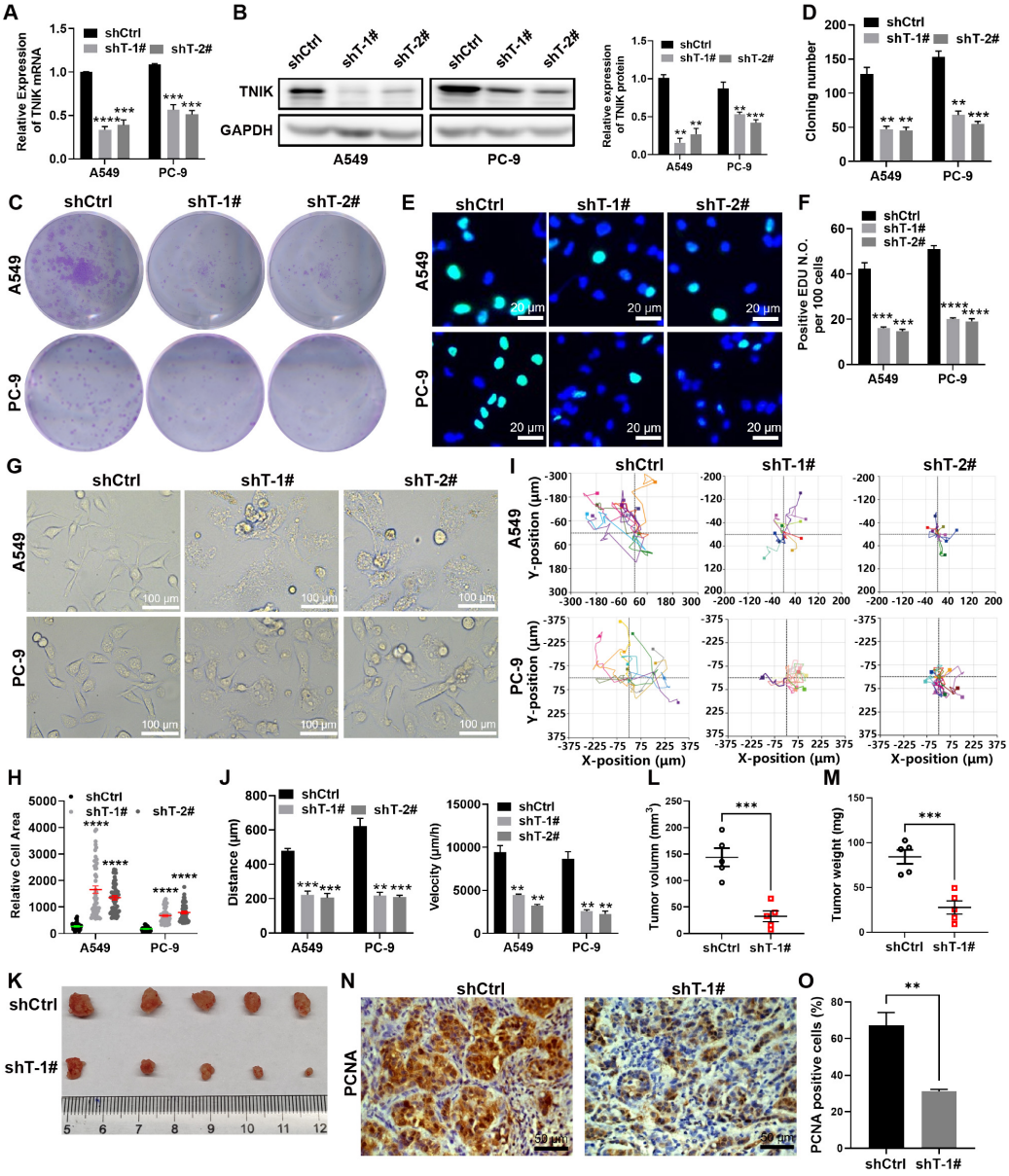

Fig. 2. TNIK knockdown suppresses the malignant phenotype of lung adenocarcinoma cells. (A) qRT-PCR analysis of TNIK knockdown efficacy. (B) Immunoblot analysis of the indicated proteins in control and TNIK knockdown A549 and PC-9 cells. The loading control was GAPDH. The TNIK expression level relative to GAPDH was standardized to control cells (n = 3 per group). (C,D) Representative images of control and TNIK knockdown A549 and PC-9 colonies and the relative colony number (n = 3 per group). (E,F) Representative images of control and TNIK knockdown A549 and PC-9 cells with EDU labeling, and the positive EDU count. Merge panels include DAPI (blue, nuclei). Scale bar, 20 μm. (G) The morphology of control and TNIK knockdown A549 and PC-9 cells. Scale bar, 100 μm. (H) The cell area was measured with Image J software, with 50 cells counted per condition. (I,J) Representative images of the migration trajectories of control and TNIK knockdown cells, and the calculated velocity and distance of cell migration. (K) Tumor xenografts from control and TNIK knockdown A549 cells. (L,M) The growth curve and weight of xenografts from control and TNIK knockdown A549 cells. (N,O) IHC staining of PCNA in control and TNIK knockdown A549 tissues, and the PCNA-positive cell count. Scale bar, 50 μm. ** $p < 0.01$, *** $p < 0.001$, **** $p < 0.0001$. shCtrl, a shRNA control; shT-1#, a shRNA of TNIK-1#; shT-2#, a shRNA of TNIK-2#; qRT-PCR, quantitative reverse transcription polymerase chain reaction; EDU, 5-ethynyl-2′-deoxyuridine; DAPI, 4′,6-diamidino-2-phenylindole; PCNA, proliferating cell nuclear antigen.

A total of 2543 genes were dysregulated in TNIK knockdown cells compared to control cells. GSEA revealed that TNIK depletion significantly inhibited the mitosis-related biological process (Fig. 3A). KEGG pathway analysis showed that dysregulated genes were involved in the cell cycle and in several cancer-related pathways, includ-

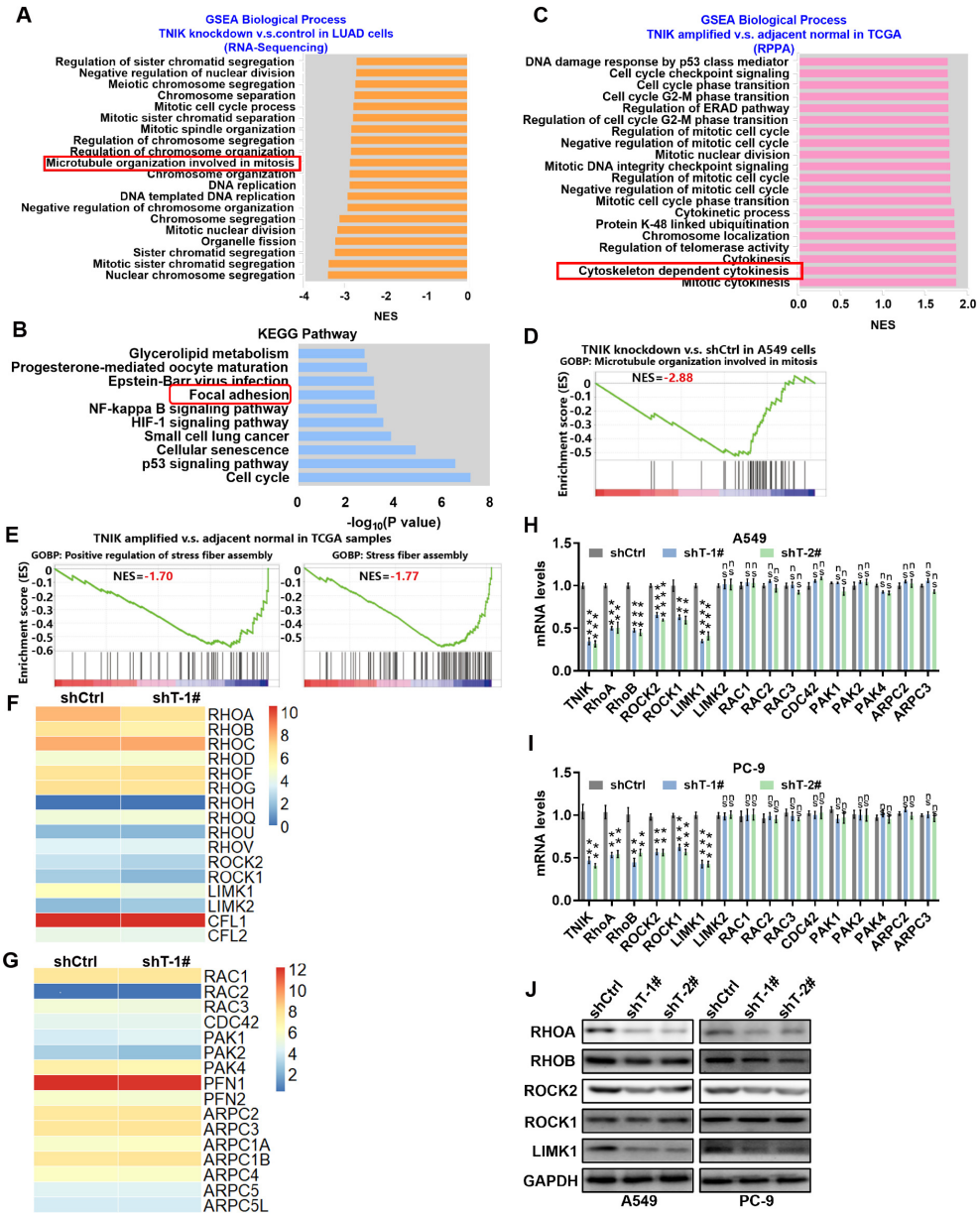

Fig. 3. TNIK regulates F-actin and microtubule cytoskeletal organization via the RHO/ROCK/LIMK1 signaling pathway. (A) The top 20 enriched gene sets identified by GSEA analysis based on the differentially expressed genes between A549 cells with stable TNIK knockdown and the control. The biological processes highlighted in the red box were associated with the cytoskeleton: microtubule organization invovled in mitosis. (B) KEGG pathway analysis based on the differentially expressed genes between A549 cells with stable TNIK knockdown and the control. The biological processes highlighted in the red box were associated with the cytoskeleton: focal adhesion. (C) Top 20 enriched gene sets identified by GSEA analysis based on the differentially expressed genes between 14 LUAD samples with high expression of TNIK detected by RPPA and 59 adjacent normal samples from the TCGA database. The biological processes highlighted in the red box were associated with the cytoskeleton: cytoskeleton dependent cytokinesis. (D) GSEA plot showing RNA-seq data from cells with stable TNIK knockdown relative to control cells. (E) GSEA plot showing TCGA data from 14 LUAD samples with high TNIK expression detected by RPPA relative to 59 adjacent normal samples from the TCGA database. (F,G) Heatmap displaying the transcript levels of indicated genes. (H,I) qRT-PCR verification of the expression of small GTPase RHO-related genes in control (shCtrl) and stable TNIK knockdown cells. Data represent the mean ± SEM. (J) Immunoblot analysis of the indicated proteins in A549 and PC-9 cells with stable TNIK knockdown or the control. "ns" indiactes $p > 0.05$ and is used to indicate no significant difference. ** $p < 0.01$, *** $p < 0.001$, **** $p < 0.0001$. GSEA, gene set enrichment analysis; KEGG, Kyoto Encyclopedia of Genes and Genomes; RHO, Ras homolog gene family; RAC, Ras-related C3 botulinum toxin substrate; ROCK, RHO-associated kinase; LIMK, LIM motif-containing protein kinase; PAK, p21-activated kinase; ARPC, actin related protein 2/3 complex.

ing p53 and the HIF-1 signaling pathway (Fig. 3B). Moreover, GSEA analysis showed that high TNIK expression detected by RPPA in TCGA LUAD samples promoted the mitosis-associated biological process (Fig. 3C). In addition, light microscopy revealed increased cell spreading in the TNIK knockdown group compared to the control group (Fig. 2G). Previous research has suggested that TNIK overexpression regulates actin assembly, thereby inducing cell spreading and causing adherent cells to round up and lose adhesion to the culture plate [13]. Cell spreading is dependent on actin filament dynamics and force generation by the FA contacts on the surface [21]. We therefore focused on the cytoskeleton-related biological process. As shown in Fig. 3A–C, the three biological processes highlighted in the red box were associated with the cytoskeleton: microtubule organization involved in mitosis, cytoskeleton-dependent cytokinesis and FA. Furthermore, we analyzed the top-ranked GSEA gene sets identified in the TNIK knockdown transcriptome of A549 cells and in LUAD samples from the TCGA database with high expression of TNIK. Other processes related to cytoskeleton organization were found, including microtubule organization and stress fiber assembly (Fig. 3D,E). The control of cell polarity and shape during cell movement and division depends on crosstalk between actin and microtubules [4], of which the RHO family of small GTPases (RHO, Rac, Cdc42) and their effectors are central players [4]. Analysis of the transcriptome profile revealed significantly lower levels of RHOA/B, ROCK 1/2 and LIMK1 in cells with TNIK silencing (Fig. 3F). In contrast, there was no difference in the level of two other small GTPases, Rac and Cdc42, between cells with TNIK knockdown and control cells (Fig. 3G). Further analysis of the RHO family and their effectors by qRT-PCR confirmed that TNIK knockdown decreased the mRNA expression of RHO/ROCK/LIMK1 (Fig. 3H,I). Moreover, Western blot analysis confirmed that RHOA/B, ROCK2 and LIMK1 protein expression were reduced upon TNIK silencing (Fig. 3J). These data strongly suggest that TNIK controls F-actin and microtubule dynamics via the RHO/ROCK2/LIMK1 signaling pathway.

3.4 TNIK Regulates Focal Adhesion Turnover and Mitosis

Microtubules and actins are essential for cell division and movement [4]. Chromosome segregation during cell division relies on properly arranged microtubules and cytokinesis during the last stages of cell division and is driven by actin filaments. However, microtubules and actin filaments also provide forces to drive changes in cell shape and migration. During these processes, FAs act as a bridge between the cytoskeleton and the ECM to direct mechanotransduction, cell migration and division [8]. The assembly and disassembly of FAs depend on microtubules and actins [6]. Active pFAK-Y397 present in FAs controls several biological processes, including cell survival, proliferation, FA turnover and migration [22]. Vinculin regulates and promotes FA assembly, but FA disassembly requires the loss or inactivation of vinculin [23].

We examined the role of TNIK in the FA dynamics of LUAD cells. Phalloidin–TRITC staining was used to identify F-actin, while vinculin immunostaining was used to mark the FAs. Stable knockdown of TNIK significantly increased the number and area of FAs ($p < 0.01$, Fig. 4A–C). Immunoblot analysis was used to further examine the expression of the FA-associated key proteins vinculin and p-FAK397. Stable knockdown of TNIK led to increased expression of vinculin and decreased expression of p-FAK397 (Fig. 4D). Additionally, TNIK knockdown was found to disturb the microtubule organization (Fig. 4E) and induce formation of syncytium ($p < 0.01$, Fig. 4F).

Next, we hypothesized that FA dynamics would be disrupted by inhibition of the RHO/ROCK/LIMK1 signaling pathway. TNIK knockdown was found to induce a low level of ROCK2 protein expression, but not ROCK1 (Fig. 3J). To test our hypothesis, we assessed the levels of p-FAK397 and vinculin protein in LUAD cells treated with siRNA targeting ROCK2 or LIMK1, respectively. Immunoblot analysis revealed that ROCK2 expression was silenced by siRNA, while ROCK2 knockdown enhanced the expression of vinculin and decreased the level of p-FAK397 (Fig. 4G and **Supplementary Fig. 1A**). Consistent with these findings, LIMK1 silencing resulted in low expression of p-FAKY397 and high expression of vinculin (Fig. 4H and **Supplementary Fig. 1B**). Additionally, LIMK1 knockdown was observed to increase the number and area of FAs (**Supplementary Fig. 2**). Taken together, these findings indicate that TNIK may control FA turnover and mitosis by affecting the dynamics of F-actin and microtubules via the RHO/ROCK2/LIMK1 signaling pathway.

3.5 TNIK Knockdown Improves the Efficacy of Chemotherapeutic Drugs in Lung Adenocarcinoma

Paclitaxel (PTX), cisplatin (DDP) and adriamycin (ADR) are common and conventional anti-cancer drugs. However, drug resistance is still a major reason for chemotherapy failure in cancer [24]. Cell adhesion to the ECM is one of the critical micro-environmental elements that drives cancer cell resistance. Multifunctional and multiprotein FA complexes are essential mechanical components that functionally and structurally regulate the cell shape and cytoplasmic signaling for cell survival, proliferation, differentiation and motility [7]. The effectiveness of any specific molecular therapy is challenging due to the considerable redundancy, intricacy and interaction between downstream signaling and FA-related receptors. In the present study, we found that TNIK silencing affected FA dynamics and cytoskeletal organization, including microtubules and F-actin. The targeting of TNIK in combination with chemotherapeutic agents may overcome drug resistance. CCK-8 assays revealed that TNIK knockdown increased the sensitivity of A549 and PC-9 cells to PTX, DDP and ADR (Fig. 5A–C). PTX had IC50 values of 3.044

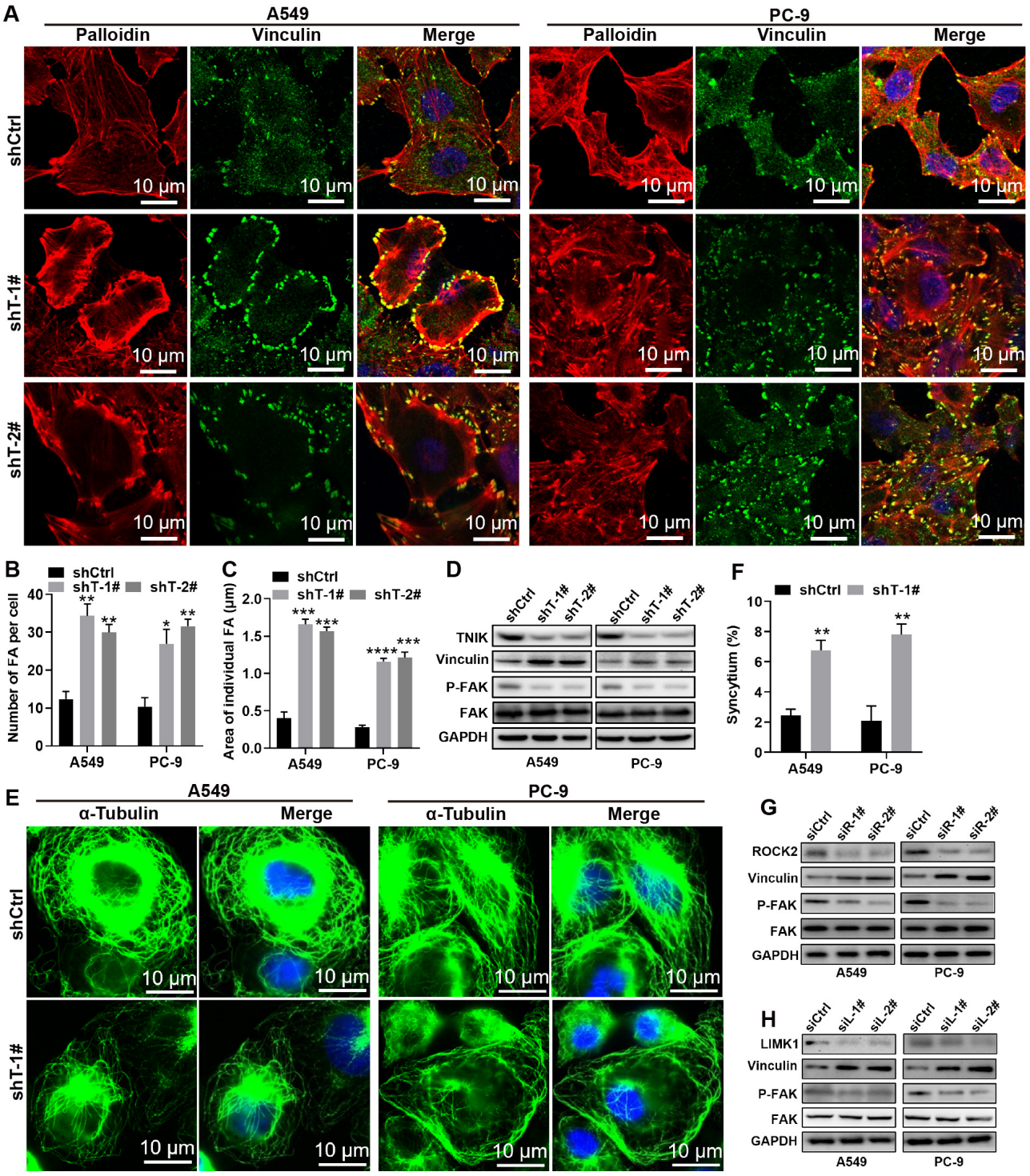

Fig. 4. TNIK regulates focal adhesion turnover and mitosis. (A) Representative images of vinculin (green) and F-actin (red) in A549 and PC-9 control and TNIK knockdown cells. Merge panels include DAPI (blue, nuclei). Scale bar, 10 μm. (B,C) Quantification of the number and average area of FAs in A549 and PC-9 control and TNIK knockdown cells. (D) Immunoblot analysis of the indicated proteins in A549 and PC-9 control and TNIK knockdown cells. (E) Immunofluorescence staining of tubulin in A549 and PC-9 control and TNIK knockdown cells. Merge panels include DAPI (blue, nuclei). Scale bar, 10 μm. (F) Statistical analysis of the syncytium ratio in the results from (E). More than 50 cells were counted per condition in each repeat. Data represent the mean ± SEM (n = 3 per group). (G) Immunoblot analysis of the indicated proteins in the A549 and PC-9 control and ROCK2 knockdown cells. (H) Immunoblot analysis of the indicated proteins in the A549 and PC-9 control and LIMK1 knockdown cells. * $p < 0.05$, ** $p < 0.01$, *** $p < 0.001$, **** $p < 0.0001$. FA, focal adhesion; FAK, focal adhesion kinase; siCtrl, a siRNA control; siR, a siRNA of ROCK; siL, a siRNA of LIMK1.

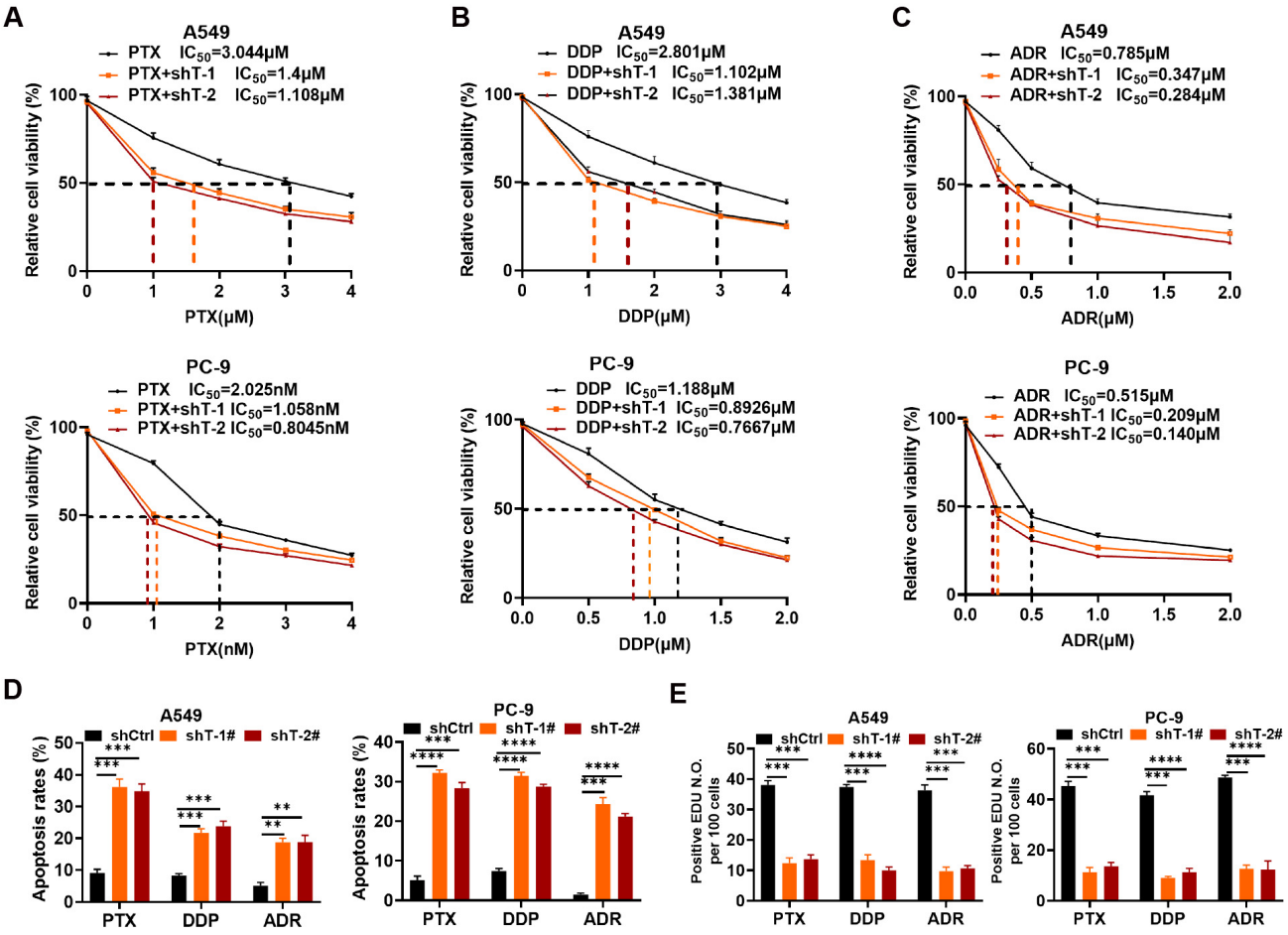

Fig. 5. TNIK knockdown improves the tumor-suppressive efficacy of chemotherapeutic drugs *in vitro*. (A–C) CCK-8 assays were used to evaluate cell viability in A549 and PC-9 cells with either stable TNIK knockdown or control vector following treatment with PTX (A), DDP (B) or ADR (C) for 48 h (n = 3 per group). (D) Cell apoptosis was analyzed by Annexin V-FITC/PI double staining of A549 and PC-9 control and stable TNIK knockdown cells after treatment with PTX (1.108 μM for A549, 0.8045 nm for PC-9), DDP (1.102 μM for A549, 0.7667 μM for PC-9), or ADR (0.284 μM for A549, 0.14 μM for PC-9) for 48 h. Results are representative of three independent experiments. (E) Cell proliferation was assessed by EDU labeling of A549 and PC-9 control and stable TNIK knockdown cells after treatment with PTX (1.108 μM for A549, 0.8045 nm for PC-9), DDP (1.102 μM for A549, 0.7667 μM for PC-9), or ADR (0.284 μM for A549, 0.14 μM for PC-9) for 48 h. ** $p < 0.01$, *** $p < 0.001$, **** $p < 0.0001$. PTX, paclitaxel; DDP, cisplatin; ADR, adriamycin; CCK-8, cell counting kit-8; PI, propidium iodide.

μM and 1.4 μM/1.108 μM in control and TNIK knockdown A549 cells, respectively (Fig. 5A), and 2.025 nM and 1.058 nM/0.805 nM in control and TNIK knockdown PC-9 cells, respectively (Fig. 5A). DDP had IC50 values of 2.801 μM and 1.102 μM/1.381 μM in control and TNIK knockdown A549 cells, respectively (Fig. 5B), and 1.188 μM and 0.893 μM/0.767 μM in control and TNIK knockdown PC-9 cells, respectively (Fig. 5B). ADR had IC50 values of 0.785 μM and 0.347 μM/0.284 μM in control and TNIK knockdown A549 cells, respectively (Fig. 5C), and 0.515 μM and 0.209 μM/0.140 μM in control and TNIK knockdown PC-9 cells, respectively (Fig. 5C). To determine whether the cytotoxicity of these drugs against A549 and PC-9 cells with TNIK knockdown was related to apoptosis, we utilized flow cytometry to measure the proportion of apoptotic cells. TNIK knockdown in A549 and PC-9 cells markedly increased the rate of apoptosis in comparison to the control group ($p < 0.01$, Fig. 5D and **Supplementary Fig. 3A**). Consistent with this finding, TNIK knockdown resulted in fewer EDU-positive cells ($p < 0.001$, Fig. 5E and **Supplementary Fig. 3B**). Together, these results indicate that TNIK knockdown improves the tumor-suppressive efficacy of chemotherapeutic drugs.

4. Discussion

The MAP4K protein from the Ste20 family is involved in various physiological and pathological processes [25]. Within this family, p21-activated kinases (PAKs) and GCKs have been shown to mediate multifaceted intracellular processes such as cell shape, cell motility and cytoskeletal rearrangement [26–30]. TNIK is a serine/threonine ki-

nase of the GCK family. As a member of the oncogenic "driver" kinome, TNIK could also serve as a potential therapeutic target [17]. Previous studies have shown that TNIK is involved in the development of gastric cancer, mammary carcinoma, colorectal cancer and LUSC [20,31–33]. In the present study, tissue chip analysis revealed that TNIK was overexpressed in LUAD and LUSC compared to adjacent normal lung tissues (Fig. 1A,B). TNIK has been documented to localize in the nucleus where it is a crucial, specific activator of the Wnt transcriptional pathway, and has therefore been proposed as a potential anticancer target [34]. Our study found that TNIK was mainly localized to the cytosol in LUAD cells, and to the nucleoplasm in adjacent normal cells and LUSC cells. We also elucidated various roles of TNIK in LUAD, including cell proliferation, movement and chemotherapy. Moreover, the mechanism by which TNIK controls FA dynamics and mitosis is through the regulation of F-actin and microtubule dynamics via the RHO/ROCK2/LIMK1 signaling pathway.

A recently published structural model offers some insight into the scaffold function of full-length TNIK [15]. The kinase domain serves as a molecular switch, while the C-terminal CNH domain has the conserved function of binding small GTPases, consistent with its role in cytoskeletal organization [13,16,35,36]. Microtubules and the actin cytoskeleton must be coordinately regulated for the cell to perform intricate biological processes, such as cell movement and division [4]. The crosstalk between microtubules and actin can be direct, or it can be mediated by signaling molecules and intermediate proteins, such as RHO GTPases [4]. These small GTPases control LIMK1 activity with the help of their effector kinase, ROCK and PAK 1 and 4 [37]. LIMK1 contributes to cytoskeletal dynamics by independently modifying actin filaments and microtubules [11,38]. In the current study, we observed that TNIK knockdown in LUAD cells resulted in an increased number and area of FAs, as well as increased area of cell spreading and inhibition of cell proliferation. Further research demonstrated that TNIK regulates microtubule organization as well as actin filaments. In addition, we found that TNIK regulates the expression of RHOA/B, ROCK2 and LIMK1 in the RHO signaling pathway. Thus, it is possible that TNIK recruits RHO, ROCK2 and LIMK1, and that its kinase domain serves as a molecular regulator of these proteins by switching them on and off [39]. RHOA has been demonstrated to contribute positively to tumor development in almost all cancer types, whereas RHOB appears to play a dual role in cancer [40]. Luis-Ravelo *et al.* [41] suggested that high RHOB levels promote metastasis and chemoresistance in LUAD. Calvayrac *et al.* [42] reported that low levels of RHOB expression in non-small-cell lung cancer correlated with a good response to EGFR-TKI treatment, whereas high levels of RHOB expression corresponded to a poor response. Consistent with these findings, we found that TNIK knockdown resulted in lower levels of RHOA and RHOB expression, as well as decreased chemoresistance. Our study uncovered a striking divergence in the subcellular localization of TNIK between LUAD and LUSC. In LUAD, TNIK predominantly localizes to the cytoplasm, whereas in LUSC, TNIK is primarily nuclear. This subtype-specific localization pattern likely reflects distinct signaling requirements critical for tumor progression. In LUAD, cytoplasmic TNIK is likely engaging cytoskeletal pathways (e.g., RHOA/ROCK2) to promote migration. Conversely, nuclear TNIK in LUSC may exert the oncogenic roles analogous to its function in colorectal cancer, where it regulates components of the β-catenin/T-cell factor-4 (TCF-4) transcriptional complex [19]. The mechanisms governing this localization dichotomy remain poorly understood but represent a compelling area for future investigation.

Chemotherapy is the traditional cancer treatment used for all types of cancer. However, chemoresistance remains a major obstacle to effective cancer treatment. More advanced cancer treatments now combine traditional chemotherapy with targeted therapy [3,7]. Our study showed that TNIK regulates F-actin and microtubule organization to control FA turnover and mitosis, suggesting that TNIK is a potential target for inhibiting cancer cell proliferation and migration. As shown in Fig. 5, targeting TNIK in combination with conventional chemotherapeutic agents significantly decreased cell viability and increased the apoptosis of LUAD cells. On the other hand, it is well known that FAK is frequently overexpressed in cancer, with several FAK inhibitors currently under development. Targeting of FAK could be especially effective in combination with other agents to reverse the serious side effects of chemotherapies or targeted therapies [8]. In conjunction with our finding that TNIK is mainly localized in the cytoplasm of LUAD cells and regulates p-FAK397 expression, the targeting of both FAK and TNIK could be an effective strategy for future molecular targeted therapies against LUAD.

5. Conclusions

Taken together, the results of this study demonstrate that TNIK regulates the dynamics of actin filaments and microtubules via the RHO/ROCK2/LIMK1 signaling axis to promote FA turnover and cell division in LUAD. Functionally, the silencing of TNIK inhibits cell movement and cell viability in LUAD. Our findings offer new insights into the development of novel treatment approaches for LUAD by combining TNIK targeting with chemotherapeutic agents.

Availability of Data and Materials

The datasets used and/or analyzed during the present study are available from the corresponding authors on reasonable request.

Author Contributions

LianZ, CZ, YW and QZ designed the research study. YL and MS contributed to the experiments and YL, MS, XH, TZ, XS, LuZ analyzed the data. LianZ wrote the manuscript. All authors contributed to editorial changes in the manuscript. All authors read and approved the final manuscript. All authors have participated sufficiently in the work and agreed to be accountable for all aspects of the work.

Ethics Approval and Consent to Participate

Shanghai OUTDO Biotech committees approved of the informed consent and the patient sample study, which followed with all applicable ethical regulations (protocol code SHYJS-CP-1901006, approved on 1st January 2019 for HLugS120CS01; protocol code SHYJS-CP-1901005, approved on 1st January 2019 for HLugA150CS03). The study was carried out in accordance with the guidelines of the Declaration of Helsinki. The Chongqing Medical University Institutional Animal Care and Treatment Committee's rules were followed in the humane treatment of all animals (Ethic Approval Number: IACUC-CQMU-2024-0593).

Acknowledgment

Not applicable.

Funding

This work was supported in part by National Natural Science Foundation of China Grants-in-aid 82173243 (to CZ), Natural Science Foundation of Chongqing Municipality Grant cstc2021jcyj-msxmX0190 (to CZ); Chongqing Postdoctoral Science Foundation Grant CSTB2023NSCQ-BHX0014 (to LZ), Chongqing Medical University, Postdoctoral start-up Foundation Grant R1063 (to LZ).

Conflict of Interest

The authors declare no conflict of interest.

Supplementary Material

Supplementary material associated with this article can be found, in the online version, at https://doi.org/10.31083/FBL38875.

References

[1] Siegel RL, Miller KD, Wagle NS, Jemal A. Cancer statistics, 2023. CA: A Cancer Journal for Clinicians. 2023; 73: 17–48. https://doi.org/10.3322/caac.21763.

[2] Herbst RS, Morgensztern D, Boshoff C. The biology and management of non-small cell lung cancer. Nature. 2018; 553: 446–454. https://doi.org/10.1038/nature25183.

[3] Yuan M, Huang LL, Chen JH, Wu J, Xu Q. The emerging treatment landscape of targeted therapy in non-small-cell lung cancer. Signal Transduction and Targeted Therapy. 2019; 4: 61. https://doi.org/10.1038/s41392-019-0099-9.

[4] Dogterom M, Koenderink GH. Actin-microtubule crosstalk in cell biology. Nature Reviews. Molecular Cell Biology. 2019; 20: 38–54. https://doi.org/10.1038/s41580-018-0067-1.

[5] Critchley DR. Focal adhesions - the cytoskeletal connection. Current Opinion in Cell Biology. 2000; 12: 133–139. https://doi.org/10.1016/s0955-0674(99)00067-8.

[6] Mavrakis M, Juanes MA. The compass to follow: Focal adhesion turnover. Current Opinion in Cell Biology. 2023; 80: 102152. https://doi.org/10.1016/j.ceb.2023.102152.

[7] Eke I, Cordes N. Focal adhesion signaling and therapy resistance in cancer. Seminars in Cancer Biology. 2015; 31: 65–75. https://doi.org/10.1016/j.semcancer.2014.07.009.

[8] Mishra YG, Manavathi B. Focal adhesion dynamics in cellular function and disease. Cellular Signalling. 2021; 85: 110046. https://doi.org/10.1016/j.cellsig.2021.110046.

[9] Kleinschmidt EG, Schlaepfer DD. Focal adhesion kinase signaling in unexpected places. Current Opinion in Cell Biology. 2017; 45: 24–30. https://doi.org/10.1016/j.ceb.2017.01.003.

[10] Lim ST, Chen XL, Lim Y, Hanson DA, Vo TT, Howerton K, *et al*. Nuclear FAK promotes cell proliferation and survival through FERM-enhanced p53 degradation. Molecular Cell. 2008; 29: 9–22. https://doi.org/10.1016/j.molcel.2007.11.031.

[11] Gorovoy M, Niu J, Bernard O, Profirovic J, Minshall R, Neamu R, *et al*. LIM kinase 1 coordinates microtubule stability and actin polymerization in human endothelial cells. The Journal of Biological Chemistry. 2005; 280: 26533–26542. https://doi.org/10.1074/jbc.M502921200.

[12] Borensztajn K, Peppelenbosch MP, Spek CA. Coagulation Factor Xa inhibits cancer cell migration via LIMK1-mediated cofilin inactivation. Thrombosis Research. 2010; 125: e323–e328. https://doi.org/10.1016/j.thromres.2010.02.018.

[13] Fu CA, Shen M, Huang BC, Lasaga J, Payan DG, Luo Y. TNIK, a novel member of the germinal center kinase family that activates the c-Jun N-terminal kinase pathway and regulates the cytoskeleton. The Journal of Biological Chemistry. 1999; 274: 30729–30737. https://doi.org/10.1074/jbc.274.43.30729.

[14] Roskoski R, Jr. A historical overview of protein kinases and their targeted small molecule inhibitors. Pharmacological Research. 2015; 100: 1–23. https://doi.org/10.1016/j.phrs.2015.07.010.

[15] Kukimoto-Niino M, Shirouzu M, Yamada T. Structural Insight into TNIK Inhibition. International Journal of Molecular Sciences. 2022; 23: 13010. https://doi.org/10.3390/ijms232113010.

[16] Taira K, Umikawa M, Takei K, Myagmar BE, Shinzato M, Machida N, *et al*. The Traf2- and Nck-interacting kinase as a putative effector of Rap2 to regulate actin cytoskeleton. The Journal of Biological Chemistry. 2004; 279: 49488–49496. https://doi.org/10.1074/jbc.M406370200.

[17] Fleuren EDG, Zhang L, Wu J, Daly RJ. The kinome 'at large' in cancer. Nature Reviews. Cancer. 2016; 16: 83–98. https://doi.org/10.1038/nrc.2015.18.

[18] Davoli T, Xu AW, Mengwasser KE, Sack LM, Yoon JC, Park PJ, *et al*. Cumulative haploinsufficiency and triplosensitivity drive aneuploidy patterns and shape the cancer genome. Cell. 2013; 155: 948–962. https://doi.org/10.1016/j.cell.2013.10.011.

[19] Yamada T, Masuda M. Emergence of TNIK inhibitors in cancer therapeutics. Cancer Science. 2017; 108: 818–823. https://doi.org/10.1111/cas.13203.

[20] Torres-Ayuso P, An E, Nyswaner KM, Bensen RC, Ritt DA, Specht SI, *et al*. TNIK Is a Therapeutic Target in Lung Squamous Cell Carcinoma and Regulates FAK Activation through Merlin. Cancer Discovery. 2021; 11: 1411–1423. https://doi.org/10.1158/2159-8290.CD-20-0797.

[21] Rangamani P, Xiong GY, Iyengar R. Multiscale modeling of cell shape from the actin cytoskeleton. Progress in Molecular Biology and Translational Science. 2014; 123: 143–167. https://doi.org/10.1016/B978-0-12-397897-4.00002-4.

[22] Alanko J, Ivaska J. Endosomes: Emerging Platforms for Integrin-Mediated FAK Signalling. Trends in Cell Biology. 2016; 26: 391–398. https://doi.org/10.1016/j.tcb.2016.02.001.
[23] Bays JL, DeMali KA. Vinculin in cell-cell and cell-matrix adhesions. Cellular and Molecular Life Sciences: CMLS. 2017; 74: 2999–3009. https://doi.org/10.1007/s00018-017-2511-3.
[24] Kannampuzha S, Gopalakrishnan AV. Cancer chemoresistance and its mechanisms: Associated molecular factors and its regulatory role. Medical Oncology (Northwood, London, England). 2023; 40: 264. https://doi.org/10.1007/s12032-023-02138-y.
[25] Garland B, Delisle S, Al-Zahrani KN, Pryce BR, Sabourin LA. The Ste20-like kinase - a Jack of all trades? Journal of Cell Science. 2021; 134: jcs258269. https://doi.org/10.1242/jcs.258269.
[26] Dan I, Watanabe NM, Kusumi A. The Ste20 group kinases as regulators of MAP kinase cascades. Trends in Cell Biology. 2001; 11: 220–230. https://doi.org/10.1016/s0962-8924(01)01980-8.
[27] Best M, Gale ME, Wells CM. PAK-dependent regulation of actin dynamics in breast cancer cells. The International Journal of Biochemistry & Cell Biology. 2022; 146: 106207. https://doi.org/10.1016/j.biocel.2022.106207.
[28] Leonhard K, Nurse P. Ste20/GCK kinase Nak1/Orb3 polarizes the actin cytoskeleton in fission yeast during the cell cycle. Journal of Cell Science. 2005; 118: 1033–1044. https://doi.org/10.1242/jcs.01690.
[29] Liu M, Lu B, Li Y, Yuan S, Zhuang Z, Li G, *et al*. P21-activated kinase 1 (PAK1)-mediated cytoskeleton rearrangement promotes SARS-CoV-2 entry and ACE2 autophagic degradation. Signal Transduction and Targeted Therapy. 2023; 8: 385. https://doi.org/10.1038/s41392-023-01631-0.
[30] LeClaire LL, Rana M, Baumgartner M, Barber DL. The Nck-interacting kinase NIK increases Arp2/3 complex activity by phosphorylating the Arp2 subunit. The Journal of Cell Biology. 2015; 208: 161–170. https://doi.org/10.1083/jcb.201404095.
[31] Yu DH, Zhang X, Wang H, Zhang L, Chen H, Hu M, *et al*. The essential role of TNIK gene amplification in gastric cancer growth. Oncogenesis. 2014; 2: e89. https://doi.org/10.1038/oncsis.2014.2.
[32] Sato K, Padgaonkar AA, Baker SJ, Cosenza SC, Rechkoblit O, Subbaiah DRCV, *et al*. Simultaneous CK2/TNIK/DYRK1 inhibition by 108600 suppresses triple negative breast cancer stem cells and chemotherapy-resistant disease. Nature Communications. 2021; 12: 4671. https://doi.org/10.1038/s41467-021-24878-z.
[33] Shitashige M, Satow R, Jigami T, Aoki K, Honda K, Shibata T, *et al*. Traf2- and Nck-interacting kinase is essential for Wnt signaling and colorectal cancer growth. Cancer Research. 2010; 70: 5024–5033. https://doi.org/10.1158/0008-5472.CAN-10-0306.
[34] Ewald CY, Pulous FE, Lok SWY, Pun FW, Aliper A, Ren F, *et al*. TNIK's emerging role in cancer, metabolism, and age-related diseases. Trends in Pharmacological Sciences. 2024; 45: 478–489. https://doi.org/https://doi.org/10.1016/j.tips.2024.04.010.
[35] Bartual SG, Wei W, Zhou Y, Pravata VM, Fang W, Yan K, *et al*. The citron homology domain as a scaffold for Rho1 signaling. Proceedings of the National Academy of Sciences of the United States of America. 2021; 118: e2110298118. https://doi.org/10.1073/pnas.2110298118.
[36] Madaule P, Furuyashiki T, Reid T, Ishizaki T, Watanabe G, Morii N, *et al*. A novel partner for the GTP-bound forms of rho and rac. FEBS Letters. 1995; 377: 243–248. https://doi.org/10.1016/0014-5793(95)01351-2.
[37] Bernard O. Lim kinases, regulators of actin dynamics. The International Journal of Biochemistry & Cell Biology. 2007; 39: 1071–1076. https://doi.org/10.1016/j.biocel.2006.11.011.
[38] Villalonga E, Mosrin C, Normand T, Girardin C, Serrano A, Žunar B, *et al*. LIM Kinases, LIMK1 and LIMK2, Are Crucial Node Actors of the Cell Fate: Molecular to Pathological Features. Cells. 2023; 12: 805. https://doi.org/10.3390/cells12050805.
[39] Kornev AP, Taylor SS. Dynamics-Driven Allostery in Protein Kinases. Trends in Biochemical Sciences. 2015; 40: 628–647. https://doi.org/10.1016/j.tibs.2015.09.002.
[40] Ju JA, Gilkes DM. RhoB: Team Oncogene or Team Tumor Suppressor? Genes. 2018; 9: 67. https://doi.org/10.3390/genes9020067.
[41] Luis-Ravelo D, Antón I, Zandueta C, Valencia K, Pajares MJ, Agorreta J, *et al*. RHOB influences lung adenocarcinoma metastasis and resistance in a host-sensitive manner. Molecular Oncology. 2014; 8: 196–206. https://doi.org/10.1016/j.molonc.2013.11.001.
[42] Calvayrac O, Mazières J, Figarol S, Marty-Detraves C, Raymond-Letron I, Bousquet E, *et al*. The RAS-related GTPase RHOB confers resistance to EGFR-tyrosine kinase inhibitors in non-small-cell lung cancer via an AKT-dependent mechanism. EMBO Molecular Medicine. 2017; 9: 238–250. https://doi.org/https://doi.org/10.15252/emmm.201606646.